ACS OMEGA

Open Access

http://pubs.acs.org/journal/acsodf

Article

Proteomic Approach Using DIA-MS Identifies Morphogenesis-Associated Proteins during Cardiac Differentiation of Human iPS Cells

Takaya Urasawa and Nana Kawasaki*

Cite This: *ACS Omega* 2025, 10, 344−357

Read Online

ACCESS | Metrics & More | Article Recommendations | Supporting Information

ABSTRACT: Human-induced pluripotent stem cell (hiPSC)-derived cardiomyocytes have potential applications in regenerative medicine. The quality by design (QbD) approach enables the efficiency and quality assurance in the manufacturing of hiPSC-derived products. It requires a molecular understanding of hiPSC differentiation throughout the differentiation process; however, information on cardiac differentiation remains limited. Proteins associated with the early stages of cardiac differentiation would be useful in the cardiomyocyte quality assessment. Here, we performed quantitative proteomics of hiPSC intermediate cells in the early phase of cardiac differentiation to better understand their molecular characteristics. Proteomic profiles suggested that day 5−7 cells were in the morphogenetic stage of cardiac differentiation. Trophoblast glycoprotein (TPBG) was the most up-regulated protein in the morphogenetic stage; it was previously shown to be up-regulated during differentiation into neural stem cells. Proteomics of TPBG-knockdown cells revealed that TPBG is involved in cell proliferation and is related to the cardiomyocyte yield, suggesting that it could be used as a marker in QbD development. Our approach helps us understand the molecular basis of hiPSC differentiation and could be a powerful tool in QbD-based manufacturing.

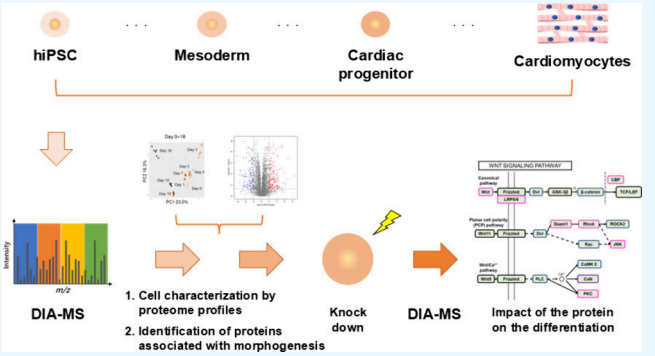

1. INTRODUCTION

Induced pluripotent stem cells (iPSC) are a type of pluripotent stem cell produced by reprogramming somatic cells. This is done by introducing several types of transcription factors, such as Oct4, Sox2, Klf4, and c-Myc.[1] Moreover iPSCs can differentiate into various tissue and organ cell types derived from three germ layers. Human-derived iPSCs (hiPSCs) have several potential applications in regenerative medicine,[2−4] drug discovery,[5−7] and disease models.[8−10] Clinical studies of hiPSC-derived cardiomyocytes are ongoing for application in diseases, such as ischemic cardiomyopathy.[11] The practical application of hiPSC-derived cardiac cells requires a sufficient supply of cells with ensured quality.[12]

Recent drug development research (including biopharmaceuticals) has been dominated by "quality by design (QbD)" development,[13] as outlined in the ICH Q8-11 guidelines.[14−17] The most important element in QbD in biopharmaceutical development is a deeper understanding of the characteristics of products and identifying critical quality attributes (CQAs) that are used to guide the control strategy and the process development.[18,19] The concept of QbD is being applied to the development of hiPSC-derived cardiomyocytes, although knowledge of the molecular basis of hiPSC differentiation remains limited, making this approach challenging. Proteins are directly involved in the cell cycle, proliferation, differentiation, and cellular function. Therefore, an understanding of changes in protein expression throughout the differentiation process is essential for QbD-based manufacturing. In particular, elucidating the changes in protein profiles during the morphogenetic stage when the distribution of numerous proteins is highly variable is essential to increase the efficiency of cardiac differentiation in the early stages, improving the yield of differentiated cells and reducing batch failure rates. Proteomics with liquid chromatography/tandem mass spectrometry (LC/MS/MS) is useful to understand the intracellular proteome profile[20] and identify the proteins associated with differentiation. However, proteomics studies of human stem cell-derived cardiomyocytes are limited to identifying marker proteins for differentiation and maturation by measuring cardiac progenitor cells[21] and postbeat cell maturation.[22] Additionally, the proteins identified using conventional data-

Received: July 9, 2024
Revised: December 6, 2024
Accepted: December 13, 2024
Published: December 30, 2024

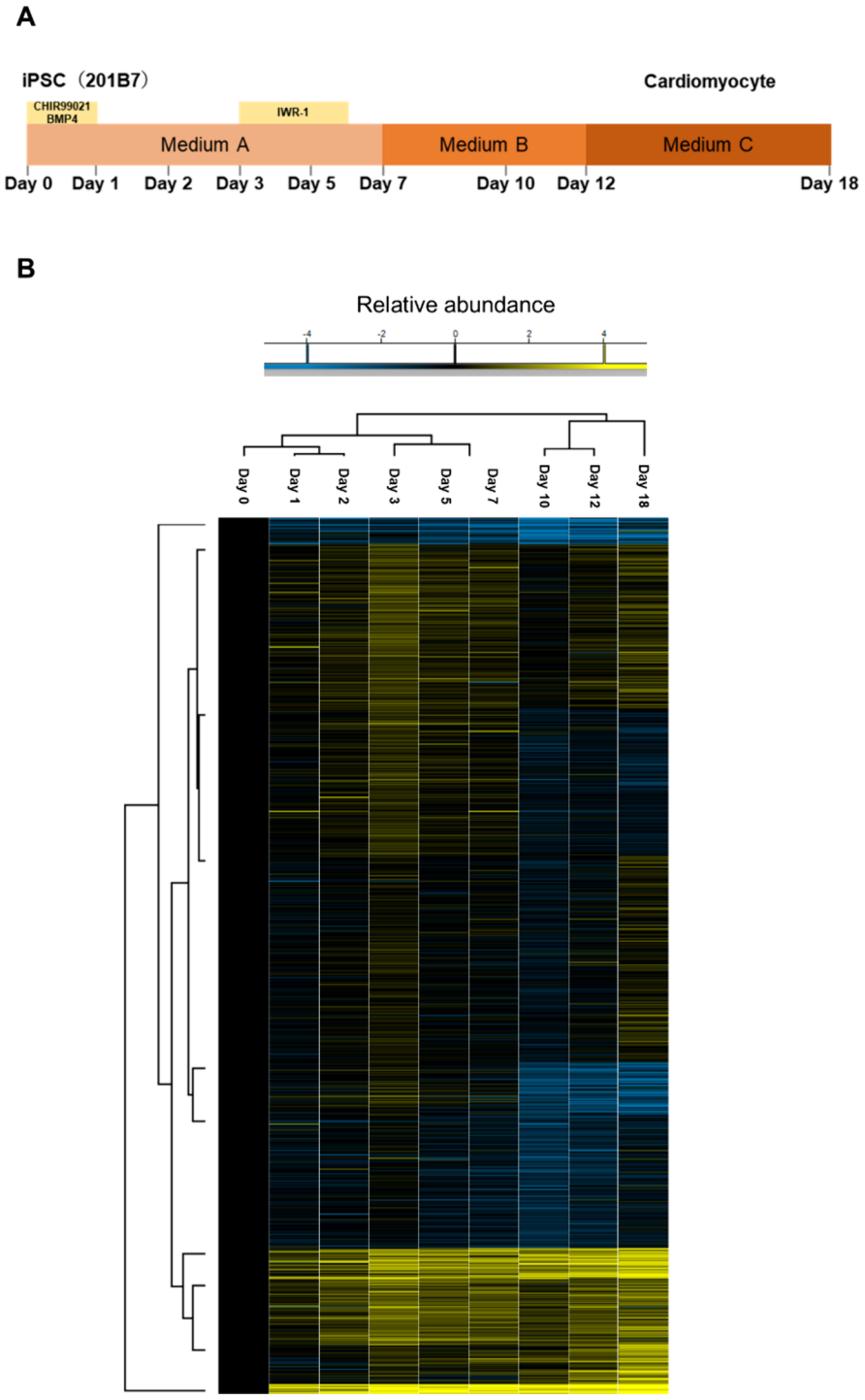

Figure 1. Proteome profiles in the early phase of cardiac differentiation. (A) Cell differentiation methods. hiPSCs were differentiated into cardiomyocytes after 18 days. On days 0−1 of differentiation, CHIR99021 was added to activate the Wnt/β-catenin pathway, and on days 3−6 of differentiation, IWR-1 was added to inhibit the Wnt/β-catenin pathway. (B) Clustering analysis with heat map using 4166 protein quantitative values (n = 6).

dependent acquisition mass spectrometry (DDA-MS) in previous studies are insufficient to understand hiPSC-derived cardiomyocytes for QbD.

Recently, data-independent acquisition mass spectrometry (DIA-MS)[23] has attracted attention as a quantitative proteomic tool owing to its ability to perform comprehensive quantitative analysis of proteins with high reproducibility. Previously, we demonstrated that DIA-MS helps understand the early phase of neuronal differentiation at the molecular level.[24] We elucidated temporal changes in the proteome profile and identified an up-regulated protein as a potential marker of neural stem cells (NSCs) using DIA-MS with a spectral library search. Lately, DIA-NN (the software for DIA-MS) allows quantitative proteomics via library-free searching;[25] this potentially facilitates simple and rapid understanding of the molecular basis of cardiac differentiation for the

https://doi.org/10.1021/acsomega.4c06371
ACS Omega 2025, 10, 344−357

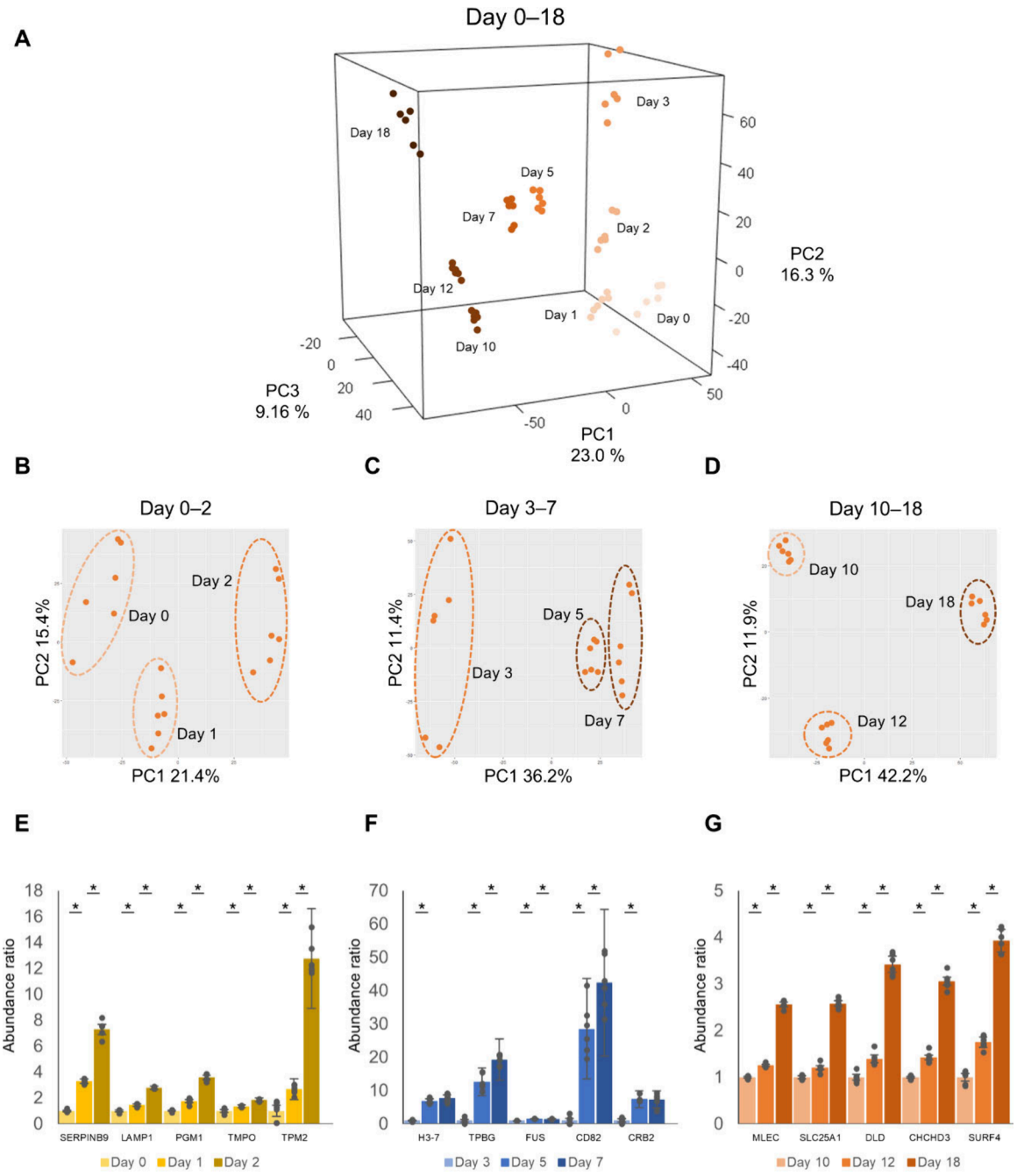

Figure 2. Characterization of the differentiation stage by PCA of the proteome profile. (A) 3D score plot of protein quantification values on days 0−18. (B) 2D score plot of protein quantification values on days 0−2. (C) 2D score plot of protein quantification values on days 3−7. (D) 2D score plot of protein quantification values on days 10−18. (E) Changes in the levels of the top 5 proteins with positive contribution to PC1 on days 0−2. SERPINB9, Serpin B9 (left); LAMP1, lysosome-associated membrane glycoprotein 1 (second left); PGM1, phosphoglucomutase-1 (middle); TMPO, lamina-associated polypeptide 2 isoform α (second right); TPM2, tropomyosin β chain (right). Each value is shown as the relative value based on the peak area of the protein on day 0. (F) Changes in the levels of the top 5 proteins with positive contribution to PC1 on days 3−7. H3-7, histone H3-7 (left); TPBG, trophoblast glycoprotein (second left); FUS, RNA-binding protein FUS (middle); CD82, CD82 antigen (second right); CRB2, protein crumbs homologue 2 (right). Each value is shown as the relative value based on the peak area of the protein on day 3. (G) Changes in the levels of the top 5 proteins with positive contribution to PC1 on days 10−18. MLEC, malectin (left); SLC25A1, tricarboxylate transport protein mitochondrial (second left); DLD, dihydrolipoyl dehydrogenase mitochondrial (middle); CHCHD3, MICOS complex subunit MIC19 (second right); SURF4, surfeit locus protein 4 (right). Each value is shown as the relative value based on the peak area of protein on day 10. Data are shown as the mean ± standard error, $n = 6$. *$p < 0.05$.

QbD approach. In this study, quantitative proteomics was performed to gain a deeper understanding of hiPSC intermediate cells in the early phase of cardiac differentiation using DIA-MS with a library-free search using DIA-NN software. Quantitative proteomics revealed temporal changes in the proteomic profile and several up-regulated proteins during morphogenesis stages. RNA interference (RNAi) and subsequent quantitative proteomics were performed to investigate the potential of the up-regulated proteins as a marker to evaluate morphogenetic cells status. Our proteomic

https://doi.org/10.1021/acsomega.4c06371
ACS Omega 2025, 10, 344−357

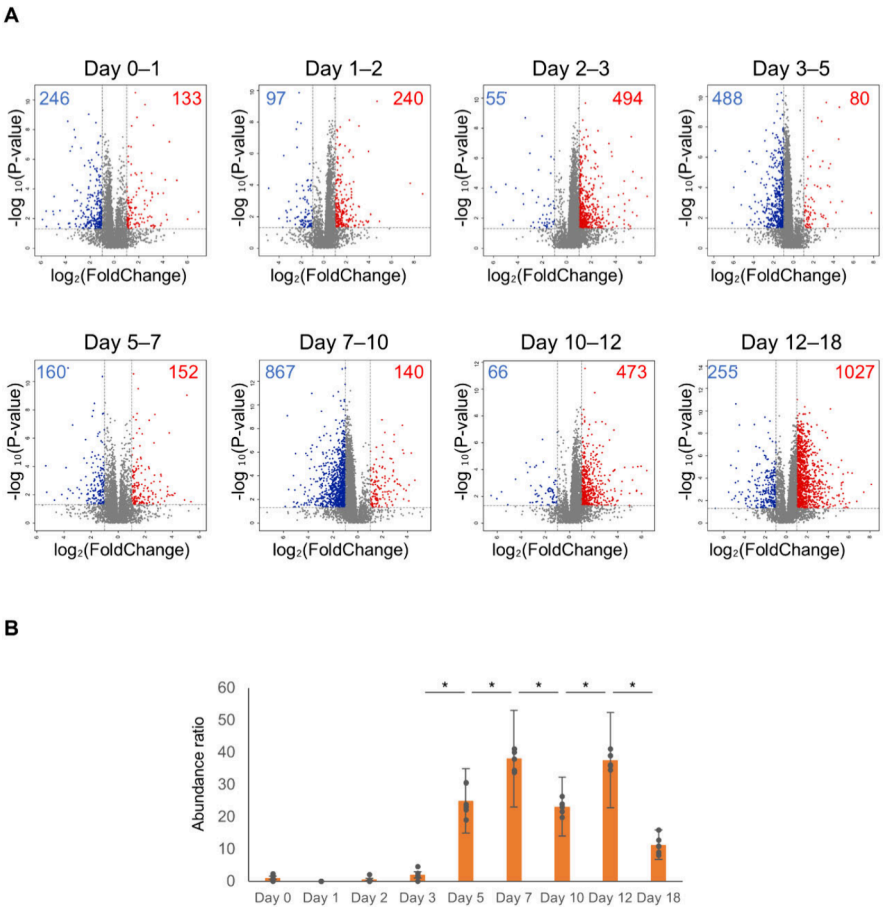

Figure 3. Extraction of up-regulated and down-regulated proteins by volcano plots. (A) Volcano plots on days 1, 2, 3, 5, 7, 10, 12, and 18 of cardiac differentiation. The points are relative to the values of the previous differentiation stage. (B) Changes in the TPBG level measured by DIA-MS. Each value is shown as the relative value based on the peak area of proteins on day 0. Data are shown as the mean ± standard error, $n = 6$. *$p < 0.01$.

approach will advance our understanding of cell differentiation at the molecular level and allow us to develop QbD-based strategies to ensure cell yield and quality.

2. RESULTS

2.1. Characterization of Cells in the Early Phase of Cardiac Differentiation by Proteome Profile. Based on a previously reported method,[12] hiPSC 201B7 cells were induced to differentiate into cardiomyocytes for 18 days (n = 6). The cells were cultured in medium A (see Experimental Methods) from days 0 to 7. On the first day, CHIR99021 was added to activate the Wnt/β-catenin pathway, while IWR-1 was added to inhibit the Wnt/β-catenin pathway on days 3−6. The cells were cultured in medium B (see Experimental Methods) on days 7−12. On days 12−18, the cardiomyocytes were purified by culturing in medium C (see Experimental Methods) (Figure 1A). The cells started beating from day 8 (Movie S1), and the beating intensity increased with further differentiation toward day 18 (Movie S2).

The cells on days 0, 1, 3, 7, 10, and 18 were immunostained using a pluripotency marker, SSEA-4, mesoderm marker, brachyury, cardiac progenitor cell marker, Nkx2.5, and cardiomyocyte marker troponin T (Figure S1A). SSEA-4-positive cells were identified only on day 0, whereas brachyury-positive cells were identified only on day 1. Some Nkx2.5-positive cells were observed on day 3 and could be seen until day 18 with consistent staining. Troponin T-positive cells were identified from day 10 onward, with the staining intensity increasing as the differentiation progressed. R10G and α-actinin staining was observed on days 0 and 18, respectively (Figure S1B). The troponin T-positive cells increased to 55% on day 12, prior to cardiac purification (Figure S1C). Similar experiments were performed with the 610B1 cell line, and similar marker staining patterns were observed (Figure S2A,B). These results indicate that cellular changes begin from early differentiation, with mesoderm-like differentiation beginning on day 1, cardiac progenitor-like differentiation after day 3, and differentiation into cardiomyocytes from day 10 onward.

Next, proteins were digested with trypsin after cells were collected and lysed on days 0, 1, 2, 3, 5, 7, 10, 12, and 18. Quantitative proteomics was performed using DIA-MS. Approximately 5560 proteins were identified at each differentiation stage from 7492 proteins (Table S1). For 4166 proteins identified at all differentiation stages, the abundance ratios between day 0 and each differentiation stage were calculated. Hierarchical clustering analysis of these proteins showed that cardiac differentiation can be broadly divided into three stages: days 0−2, days 3−7, and days 10−18, which corresponded to culturing time in medium A with Wnt/β-catenin pathway activator, medium A with Wnt/β-catenin pathway inhibitor, and medium B/C, respectively (Figure 1B). Even though all replications were reflected, the data were clustered by differentiation days (Figure S3). Evaluation of the

https://doi.org/10.1021/acsomega.4c06371
ACS Omega 2025, 10, 344−357

Table 1. List of Cell Surface Proteins That Were Up-Regulated on Day 7 Related to Day 0[a]

ID	protein name	fold change	p-value	protein expression in NSC
Q13641	Trophoblast glycoprotein	38.05	6.19×10^{-8}	+
Q9Y639	Neuroplastin	18.51	4.82×10^{-4}	−
P51654	Glypican-3	18.38	1.19×10^{-3}	+
Q8NG11	Tetraspanin-14	16.80	3.46×10^{-4}	−
Q08722	Leukocyte surface antigen CD47	12.47	7.38×10^{-4}	−
P11532	Dystrophin	8.75	7.76×10^{-5}	−
Q8N158	Glypican-2	8.06	4.82×10^{-4}	−
P08648	Integrin alpha-5	7.9	2.52×10^{-4}	+
Q9Y625	Glypican-6	5.21	1.01×10^{-2}	−
O75581	Low-density lipoprotein receptor-related protein 6	4.23	4.38×10^{-3}	−
P19022	Cadherin-2	Day 7 only	4.96×10^{-4}	+
P54764	Ephrin type-A receptor 4	Day 7 only	5.14×10^{-6}	+
P98172	Ephrin-B1	Day 7 only	8.14×10^{-6}	+
Q01974	Tyrosine-protein kinase transmembrane receptor ROR2	Day 7 only	8.91×10^{-6}	+
Q8TCZ2	CD99 antigen-like protein 2	Day 7 only	6.17×10^{-7}	+
P01130	Low-density lipoprotein receptor	Day 7 only	1.67×10^{-2}	−
P53708	Integrin α-8	Day 7 only	2.16×10^{-3}	−
P57087	Junctional adhesion molecule B	Day 7 only	9.14×10^{-2}	−
P61073	C-X-C chemokine receptor type 4	Day 7 only	1.34×10^{-3}	−
Q03167	Transforming growth factor β receptor type 3	Day 7 only	6.41×10^{-5}	−
Q04721	Neurogenic locus notch homolog protein 2	Day 7 only	5.58×10^{-3}	−
Q13433	Zinc transporter ZIP6	Day 7 only	4.69×10^{-3}	−
Q9H6X2	Anthrax toxin receptor 1	Day 7 only	4.12×10^{-2}	−

[a]Cell surface proteins that were up-regulated on day 7 of neuronal differentiation were referred to pervious reports.[24] Day 7 only, proteins identified only on day 7. +, significantly increased proteins in NSC differentiation; −, not significantly increased (or decreased) proteins in NSC differentiation.

changes in the proteome profile across the three stages demonstrated that the proteome profile represents the status of the differentiating cells.

2.2. Selecting the Proteins Associated with the Morphogenetic Stage. To characterize the stages of cardiac differentiation, we performed principal component analysis (PCA) using the 7492 protein profile data from days 0−18 (Figure 2A, Table S2). On days 0−18, PC1 separated the prebeat cells on days 0−7 and postbeat cells on days 10−18 (23.0%). Days 5 and 7 were the turnaround points for PC2 (16.3%). In PC3, days 5 and 7 were also the turning points that divided days 0−18 into days 0−3 and days 10−18 (9.16%). These results suggest that the cell status changed significantly between days 5 and 7.

Based on the results of hierarchical clustering analysis, we also performed PCA on days 0−2, 3−7, and 10−18, and observed segregation in the PC1 direction as differentiation progressed (Figure 2B−D, Table S2). The top five proteins that positively contributed to PC1 variation were extracted (Figure 2E−G). On days 0−2, these proteins were mainly lysosomal and nuclear proteins, whereas on days 10−18, they were primarily mitochondrial proteins. The proteins extracted on days 3−7 were CD82 antigen (CD82), a cardiac progenitor cell marker,[26] and TPBG, an inhibitor of the Wnt/β-catenin pathway.

To identify the proteins that were significantly altered at each day of differentiation, volcano plots were generated based on the relative p-values and ratios of proteins in cells on days 1, 2, 3, 5, 7, 10, 12, and 18 to those in cells harvested the respective day before. Each differentiation day had a criterion of >2- or <0.5-fold change (Figure 3A, Table S3). We performed gene ontology (GO) analysis on the proteins whose expressions increased or decreased (Figures S4 and S5). On day 3, terms related to cell cycles were enriched at the top, while terms related to morphogenesis were enriched on days 5 and 7. Cytoskeletal related terms (such as actin filaments, which are important for cardiomyocytes) were enriched on day 7. Muscle structure development and mitochondrial proteins were enriched on days 10−18 and day 18, respectively. Although the day 7 cells did not show beating and were negative for troponin T staining, the proteome profile suggested morphological changes to cardiomyocytes in the stage. After day 10, the proteins whose expressions decreased were enriched in cell division and the cell cycle. Days 5 and 7 were the turning points at pre- and postbeating cells, and cell morphogenesis was in progress according to PCA and GO analysis. These results suggested that the cells on day 7 were considered critical intermediate cells, leading to proper cardiac differentiation. A network analysis was performed to characterize the proteins up-regulated in the morphogenesis stage (Figure S6A,B). Proteins whose expressions increased on day 5 formed a network centered on proteoglycans, such as syndecans and glypicans, which are involved in signal transduction of many growth factors, including Wnt, transforming growth factor-β, hedgehog, and fibroblast growth factors. On day 7, the levels of proto-oncogene tyrosine-protein kinase Src (SRC), which is known to promote cell proliferation[27,28] and migration,[29] forming a network.

Cell surface proteins are considered useful markers for the simple and rapid evaluation of intermediate cells. Proteins identified using UniProt as "cell surface" and "cell membrane" based on GO annotation and subcellular location, respectively, were selected for the morphogenesis-related proteins among the proteins whose expressions increased on day 7 related to day 0 (Tables 1 and S3). TPBG was unexpectedly identified as a candidate protein that could be used to evaluate the cells in

https://doi.org/10.1021/acsomega.4c06371
ACS Omega 2025, 10, 344−357

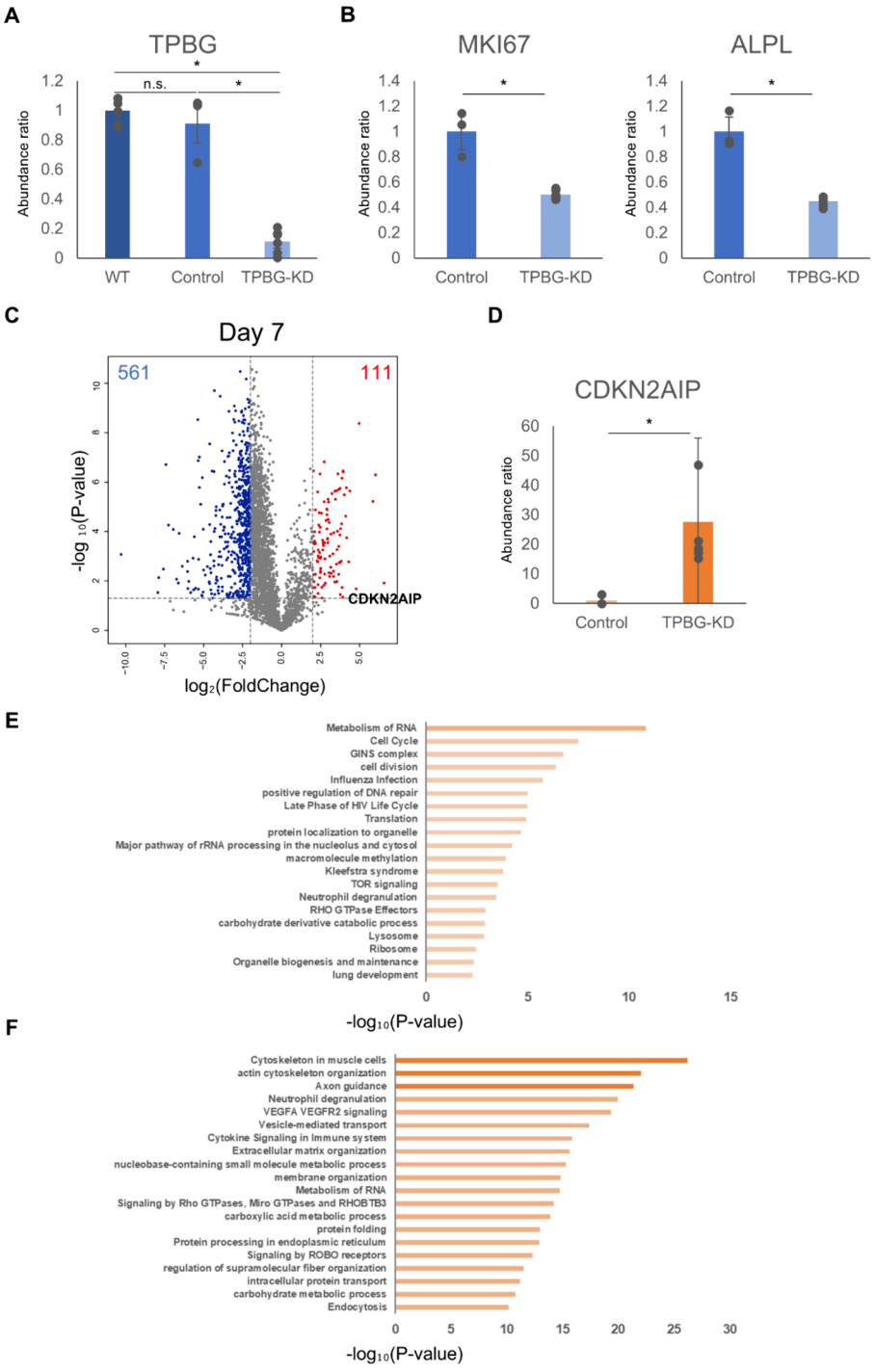

Figure 4. Effect of TPBG-KD on cardiac differentiation. TPBG-siRNA was transfected on days 5 and 6. Quantitative proteomics was performed on day 7 using DIA-MS with a library-free search. (A) Relative abundance of TPBG on day 7. (B) Relative abundance of proliferation marker protein Ki-67 (MKI67) (left) and alkaline phosphatase (ALPL) (right). (C) Comparative volcano plot for control and TPBG-KD cells on day 7. (D) Relative abundance of CDKN2A-interacting protein (CDKN2AIP) on day 7. (E) GO analysis results showed that proteins increased by TPBG-KD on day 7. (F) GO analysis results of proteins decreased by TPBG-KD on day 7. Each value is shown as the relative value based on the peak area of protein in control on day 7. Data are shown as the mean ± standard error, WT; $n = 6$, control; $n = 3$, TPBG-KD; $n = 6$. *$p < 0.05$. n.s., not significant.

the morphogenetic stage of cardiac differentiation based on the marker requirements and the most up-regulated protein in PCA and volcano plots. It was most elevated during differentiation into NSCs in our previous study.[24] Its expression rapidly increased after day 3 during cardiac differentiation and was approximately 38-fold higher on day 7 than on day 0 (Figure 3B). TPBG was expressed in most Nkx2.5-positive cells (Figure S7), indicating that it was highly expressed in cardiac progenitor cells. These results suggest that TPBG is crucial for hiPSC differentiation into ectodermal and mesodermal lineages. Immunostaining with TPBG was performed on 201B7 cells and 610B1 cells to confirm that

https://doi.org/10.1021/acsomega.4c06371
ACS Omega 2025, 10, 344−357

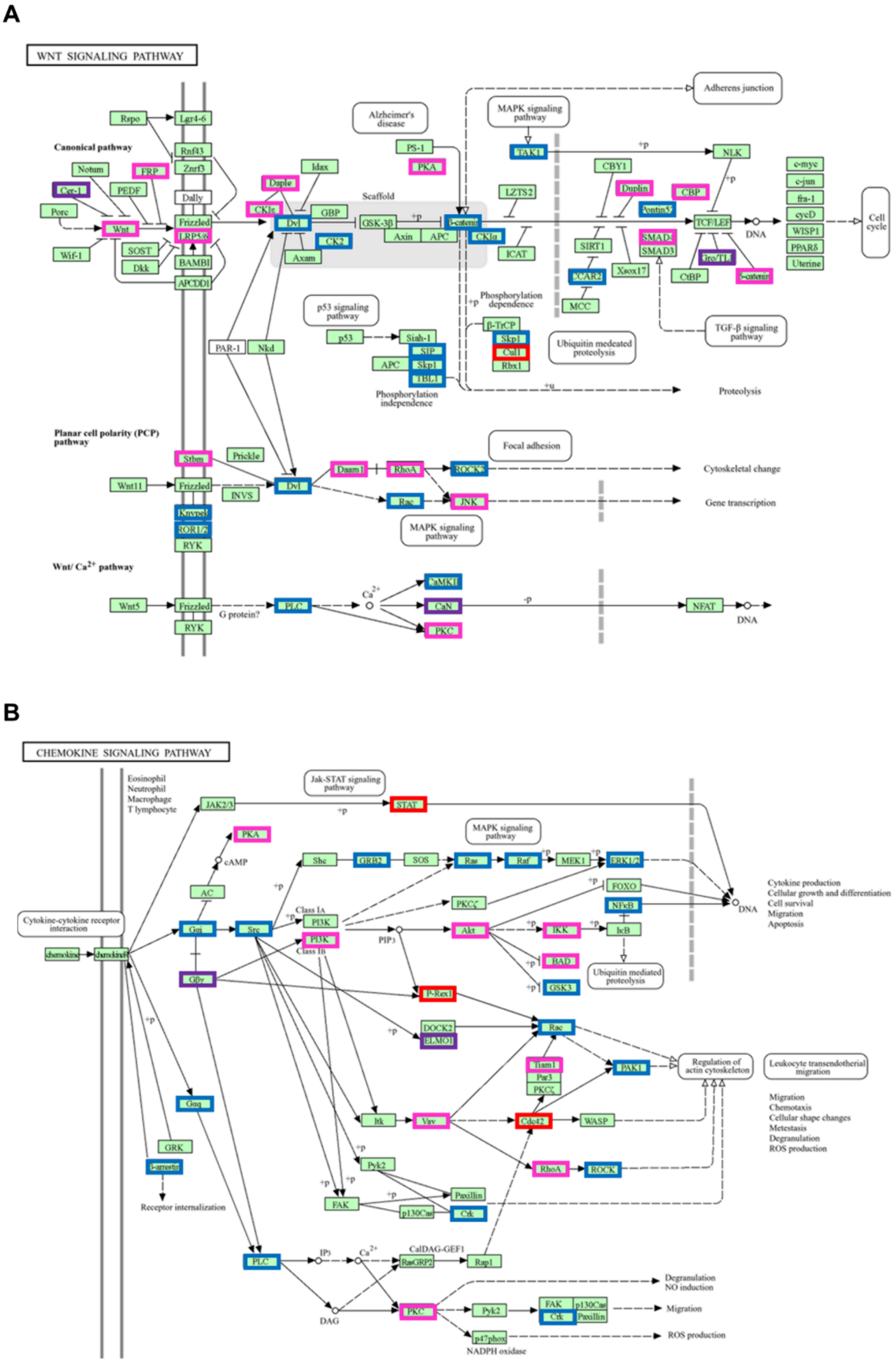

Figure 5. Analysis of the effects of TPBG-KD on signaling pathways using KEGG. (A) Wnt signaling pathway. (B) Chemokine signaling pathway. Red, increased proteins; blue, decreased proteins; pink, identified proteins only in TPBG-KD cells; purple, identified proteins only in control cells.

https://doi.org/10.1021/acsomega.4c06371
ACS Omega 2025, 10, 344−357

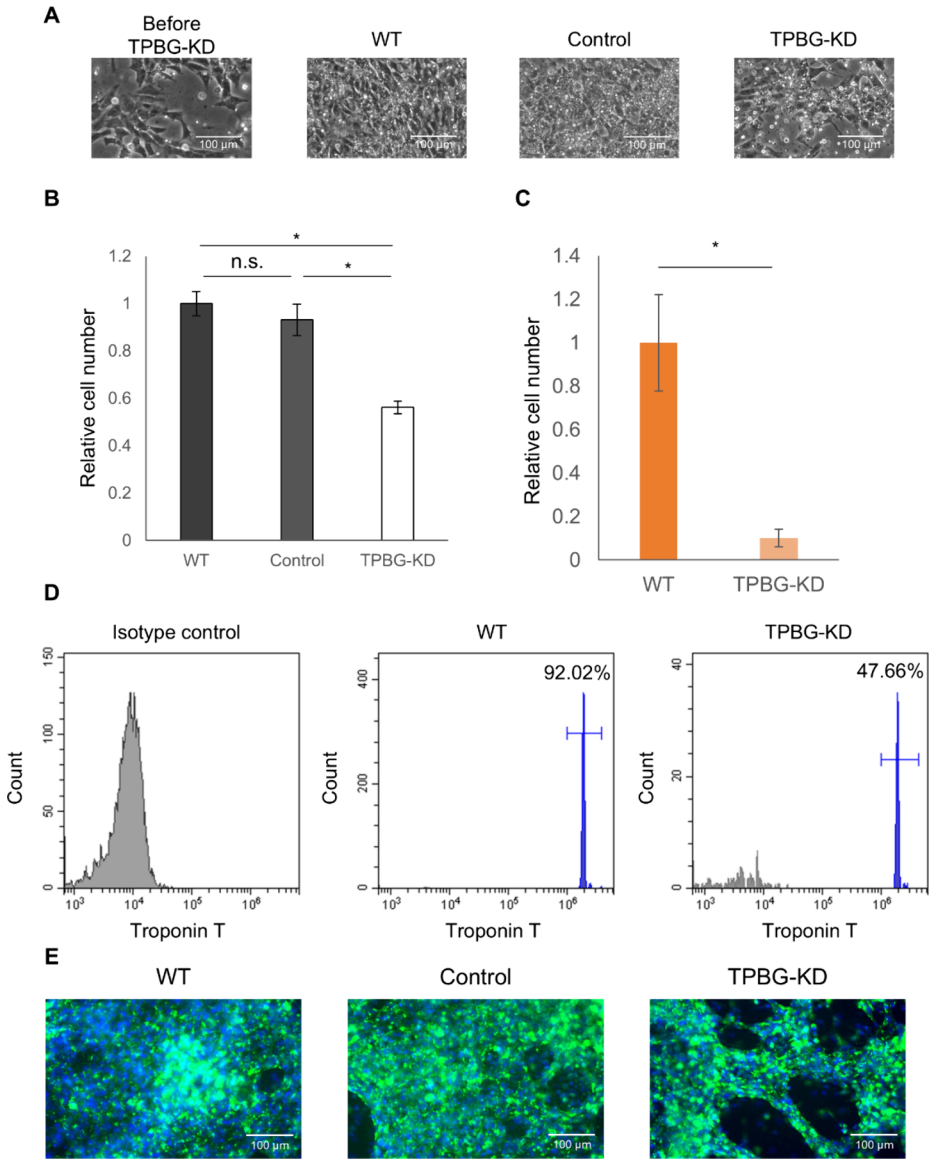

Figure 6. Effects of TPBG-KD on cell proliferation and differentiation in cardiac differentiation of hiPSCs on days 5 and 6. (A) Microscopy images of cells. Cells before TPBG-KD on day 5 (left), WT (middle left), control (middle right), TPBG-KD (right). (B) Relative cell numbers on day 6. Each value is shown as the relative value based on the number of cells in WT. Data are shown as the mean ± standard error, $n = 3$. (C) Relative troponin T-positive cell number on day 18. Data are shown as the mean ± standard error, $n = 3$. (D) Representative flow cytometry analysis for troponin T-positive cell on day 18. Isotype control (left), WT (middle), TPBG-KD (right), unstained cells (gray), troponin T-positive cells (blue). (E) Immunocytochemical analysis on day 18 for troponin T (green). Blue staining indicates DAPI signals. WT, wild type; control, nontarget siRNA; KD, knockdown; $*p < 0.05$; n.s., not significant.

the increase in TPBG expression was neither cell-line-dependent nor limited to LC/MS/MS measurements (Figure S8). The results showed that the number of stained cells rapidly increased from day 3 to 7, while TPBG signals were absent on day 1, consistent with the quantitative proteomics results using DIA-MS. This suggested that an increase in TPBG expression during cardiac differentiation was a cell line-independent phenomenon.

2.3. Impact of TPBG on the Proliferation and Differentiation of hiPSCs in Cardiac Differentiation. To assess the impact of TPBG on the morphogenetic stage of cardiac differentiation, TPBG-knockdown (KD) was performed with TPBG-siRNA on days 5 and 6 when TPBG was increased. Then, wild type (WT) cells, nontargeting siRNA transfected (control) cells and TPBG-KD cells on day 7 were solubilized and digested with trypsin. Quantitative proteomics was performed using DIA-MS with the digested protein (0.1 μg) from each cell sample (WT, $n = 6$; control, $n = 3$; TPBG-KD, $n = 6$). Transfection of nontargeted siRNA and TPBG-siRNA reduced expression to levels of 0.9 (not significant) and 0.2 ($p < 0.05$) on day 7, respectively, compared to expression in WT cells (Figure 4A). The effect of TPBG-KD on proliferation and cardiac differentiation was also evaluated by comparing the levels of marker proteins between the control cells and TPBG-KD cells. The levels of the proliferation marker protein Ki-67 (MKI67) and stem cell maker alkaline phosphatase (ALPL) were reduced to a level of 0.5 (Figure 4B). Next, proteins that were up- and down-regulated by TPBG-KD were extracted from volcano plots (Figure 4C, Table S4), and GO analysis was performed using the proteins

https://doi.org/10.1021/acsomega.4c06371
ACS Omega 2025, 10, 344−357

showing a >4- or <0.25-fold change ($p < 0.05$). The up-regulated protein, which had increased significantly, was CDKN2AIP-interacting protein (CDKN2AIP), which has been reported to inhibit cell proliferation when overexpressed (Figure 4D).[30] Up-regulated proteins included those involved in metabolism of RNA and the cell cycle, including several proteins associated with cell mitosis and cell cycle regulation (Figure 4E, Table S5). Down-regulated proteins involved those found in the cytoskeleton in muscle cells and actin cytoskeleton organization (Figure 4F, Table S5). These results suggested that the cell cycle and morphogenesis of cardiomyocytes were suppressed in TPBG-KD cells.

TPBG is reported to inhibit the Wnt/β-catenin signaling pathway and enhance the C-X-C motif chemokine 12 (CXCL12)/C-X-C chemokine receptor type 4 (CXCR4) pathway.[31−34] The intercellular level of β-catenin was reduced by TPBG-KD (Figure S9A). Kyoto Encyclopedia of Genes and Genomes (KEGG) pathway analysis revealed that TPBG-KD down-regulated not only β-catenin but also other Wnt/β-catenin pathway-associated proteins, such as dishevelled segment polarity protein 2 (DVL2), and S-phase kinase-associated protein 1 (SKP1) (Figure 5A). In contrast, CREB-binding protein (CREBBP), which is involved in the cell cycle regulation, cullin-1 (CUL1) which is associated with proteolysis, and low-density lipoprotein receptor-related protein 6 (LRP6) (Figure S9B) were up-regulated by TPBG-KD. In the CXCL12 pathway, TPBG-KD reduced SRC (Figure S9C) and its downstream proteins such as mitogen-activated protein kinase 1 (MAPK1) (Figure 5B). Our findings suggest that suppressing TPBG expression affects the cell cycle and ultimately suppresses stem cell proliferation. As many studies have shown that Wnt signaling and chemokine pathways are critical pathways for stem cell differentiation through the regulation of cell cycle and differentiation, TPBG, which is associated with both pathways, could be considered a key protein to produce hiPSC-derived cardiomyocytes.

The effects of TPBG-KD on cell proliferation and cardiac differentiation during the morphogenetic stage was examined by flow cytometry and immunostaining. On day 6, no significant differences in cell proliferation were observed between WT cells and control cells, but the number of TPBG-KD cells was significantly reduced to about 40% compared to that of the other two experimental groups (Figure 6A,B). The effect of TPBG-KD on cardiac differentiation was assessed by continuing the differentiation until day 18. Fewer beating cells were observed in TPBG-KD cells than in WT cells and control cells (Movie S3, Movie S4, Movie S5, respectively). Flow cytometry of cardiomyocytes on day18 showed significantly fewer troponin T-positive cells in TPBG-KD cells than in WT cells (Figure 6C). The percentage of troponin T-positive cells on day 18 was 83.8% ($n = 3$) for WT cells and 32.3% ($n = 3$) for TPBG-KD cells (Figure 6D). Visualization by immunostaining also showed that TPBG-KD reduced troponin T-positive cells compared with WT cells and control cells (Figure 6E). This suggests that TPBG expression in the morphogenetic stage contributes to cell proliferation in the process of cardiac differentiation.

3. DISCUSSION

3.1. Extraction of Proteins Associated with Morphogenesis during Cardiac Differentiation. In this study, DIA-MS was used to better understand the molecular characteristics of the hiPSC intermediate cells during cardiac differentiation, which is necessary for QbD-based manufacture of hiPSC-derived cardiomyocytes. In particular, quantitative proteomics by dividing early differentiation into daily stages was performed, as understanding the change in protein expression during the early phase of differentiation will lead to more efficient cardiac differentiation and fewer batch failures. Protein expression changes suggested that the cells on day 7 were undergoing morphological changes and are in the preliminary cardiac differentiation stage. We assumed that the cells on day 7 were the critical intermediates in manufacturing and selected proteins that can be used to evaluate the intermediate cell status. Proteins characterizing cells at days 3−7 of differentiation were extracted using PCA. Volcano plots and GO analysis were also used to extract proteins that increased in level on days 5−7 and are associated with morphogenesis. We also considered that cell surface proteins are preferable as differentiation marker proteins. Overall, TPBG was unexpectedly selected as the protein to evaluate critical intermediate cells for cardiac differentiation. In our previous study, TPBG was up-regulated in NSCs, and TPBG-KD promoted neuronal differentiation, suggesting that TPBG may inhibit neuronal differentiation. The results of proteomics in cardiac differentiation suggest that TPBG is also an essential protein in morphogenesis during the cardiac differentiation of hiPSCs. The importance of TPBG in endodermal differentiation of hiPSCs has not been explored in previous studies.[35,36] Future detailed analysis of endodermal differentiation will provide a comprehensive understanding of TPBG functions. Although the role of TPBG in stem cell differentiation is poorly understood, it suppresses the Wnt/β-catenin pathway by inhibiting the internalization of LRP6,[37,38] a significant component of the LRP5/LRP6/Frizzled complex, a Wnt receptor.[39] While the Wnt/β-catenin pathway promotes early cardiac differentiation,[40] it also inhibits late cardiac differentiation.[40−44] In this study, TPBG was increased on days 3−7, the period when the Wnt/β-catenin pathway inhibitor was added to the medium. TPBG is also involved in CXCL12-mediated chemotaxis in differentiating embryonic stem cells and regulating cell adhesion, cytoskeletal organization, and mobility by promoting functional CXCR4 expression.[31−34] Only a few reports have characterized protein expression during the early phase of hiPSC cardiac differentiation.[45] Previous transcriptome analysis revealed that CD82 is up-regulated on days 3, 4, and 5 during cardiac differentiation of hiPSCs.[26] In addition, flow cytometry revealed that CD82 expression began to increase on day 5 and was highest on day 7. Our proteomic approach also showed that CD82 protein increased on day 5 (Figure 2F), although the expression level was low (Table S3). Interestingly, both CD82 and TPBG are involved in the Wnt/β-catenin pathway.

3.2. The Potential of TPBG as a Marker for Intermediate Cells in Cardiac Differentiation. The effect of TPBG-KD on the morphogenetic stage of cardiac differentiation was investigated through quantitative proteomics of TPBG-KD cells and control cells. In chemokine pathways, TPBG-KD decreased the expression of SRC, which was the center in network analysis on day 7 (Figure 5B, Figure S9C). SRC promotes the nuclear translocation of β-catenin by phosphorylating it,[46] thereby activating the Wnt/β-catenin pathway and increasing cyclin D expression which involved in cell cycle.[47,48] Thus, the reduction of SRC by TPBG-KD may affect many proteins involved in the cell cycle. The effects of TPBG-KD on protein expression involved in cell proliferation

https://doi.org/10.1021/acsomega.4c06371
ACS Omega 2025, 10, 344−357

were also supported by flow cytometry experiments. TPBG-KD on days 5 and 6 reduced the number of total cells on day 6 (Figure 6B) and troponin T-positive beating cells on day 18 (Movies S3, S4, and S5, Figure 6C,D). The manufacturing of cellular products requires a sufficient supply of desired cells. Considering that TPBG may regulate proliferation during stem cell morphogenesis, using TPBG expression as a marker may be useful for monitoring the proliferative potential of the target cells and reducing batch failure. TPBG is also expressed in undifferentiated hiPSCs; however, as shown in Figure 3B, a significant 40-fold increase was observed on day 7 compared with that on day 0. This difference in expression levels is sufficient to distinguish between undifferentiated and differentiated cells. TPBG is an abundant cell surface protein that can be easily used to fractionate target cells[26] and evaluate the manufacturing process. However, TPBG alone is not sufficient to assess the proper differentiation. Therefore, time point-specific markers should also be used in combination with TPBG. In addition to TPBG, the cell surface proteins found to be specifically increased in cardiac differentiation in this study can be used more conveniently as markers for mesoderm and cardiac progenitor cells than existing nucleoproteins such as brachyury or MIXL[49] and trace proteins including ROR1/CD13.[50]

In QbD-based manufacturing of hiPSC-derived products, identification of CQAs is crucial as well as understanding of hiPSC intermediates and differentiated cells. Proteins up-regulated during the morphogenesis stage, whether common to neural or cardiac-specific, may play an important role in hiPSC differentiation and may be candidates for CQA to produce hiPSC-derived cardiomyocytes. To determine the criteria for their use in QbD-based manufacturing, proteins identified as CQA candidates need to be comprehensively investigated via various batch analyses, including worst-case scenarios and scaled-up conditions.

4. CONCLUSIONS

DIA-MS allowed for a simple and rapid understanding of temporal changes in the proteome profile and cell states at the molecular level in the early phase of hiPSC cardiac differentiation. Proteins associated with morphogenesis were increased in cells on days 5−7, suggesting that these cells are critical intermediates in cardiac differentiation. TPBG was the most up-regulated cell surface protein on day 7 and was involved in cell cycle regulation during morphogenesis. TPBG may be used as a marker of the cells in the morphogenetic stage of cardiac differentiation and be useful for cardiomyocyte yield and for ensuring quality. We believe that our approach will be useful in QbD-based manufacturing through an understanding of hiPSC derivatives and extracting potential CQAs.

5. EXPERIMENTAL METHODS

5.1. hiPSC Culture and Differentiation into Cardiomyocytes. The human iPS cell lines, iPSC 201B7 (HPS0063; CELLBANK, Ibaraki, Japan) and iPSC 610B1 (HPS0331; CELLBANK), were cultured on Geltrex (Thermo Fisher Scientific, Waltham, MA, USA)-coated six-well plates (TPP Techno Plastic Products AG Int., Klettgau, Switzerland) in Essential 8 medium (Thermo Fisher Scientific) at 37 °C in an atmosphere with 5% CO_2.

Cardiac differentiation of hiPSCs was based on the method described by Tohyama et al.[12] For cardiac differentiation, 80% confluent hiPSCs were cultured in medium A comprising RPMI1640 (FUJIFILM Wako Pure Chemical, Osaka, Japan) and B27 minus insulin (Thermo Fisher Scientific) at 37 °C in 5% CO_2 for 0−7 days. The medium was changed every 24 h. On day 0, cells were cultured in medium A containing 8 μM CHIR99021 (FUJIFILM Wako Pure Chemical) and 1 ng/mL BMP4 (FUJIFILM Wako Pure Chemical). On days 3−6, cells were cultured in medium A containing 5 μM IWR-1 (FUJIFILM Wako Pure Chemical). On day 7, cells were cultured in medium B comprising 95% α-MEM (Nacalai Tesque, Kyoto, Japan) and 5% FBS (Thermo Fisher Scientific) for 5 days. The medium was changed on day 10.

For cardiac purification, cells on day 12 were cultured in medium C,[51] which consisted of RPMI1640 (no glucose) (FUJIFILM Wako Pure Chemical), 1% CDM3 supplement with human recombinant albumin (FUJIFILM Wako Pure Chemical), L-ascorbic acid 2-phosphate (FUJIFILM Wako Pure Chemical), and 4 mM L-lactic acid (FUJIFILM Wako Pure Chemical) for 6 days. The medium was changed on day 15.

5.2. Immunofluorescence. The cells were washed twice with DPBS (−) (Nacalai Tesque), and the supernatant was removed. Next, 4% paraformaldehyde (FUJIFILM Wako Pure Chemical) was added to the cells and incubated for 10 min, followed by incubation with 0.1% saponin for 5 min. The solution was then replaced with DPBS (−) containing 3% BSA (Nacalai Tesque) and incubated for 1 h. The supernatant was removed, and the cells were incubated with primary antibodies at 4 °C for 16 h. The antibodies used were as follows: antistage-specific embryonic antigen-4 (SSEA-4) antibody (1/500; MA1-021; Thermo Fisher Scientific), antibrachyury antibody (1/40; PA5-46984; Thermo Fisher Scientific), anti-Nkx2.5 antibody (1/500; PA5-85215; Thermo Fisher Scientific, 1/33; H00001482-M04; Thermo Fisher Scientific), anticardiac troponin T antibody (1/100; MA5−12960; Thermo Fisher Scientific), anti-TPBG antibody (1/100; PA5-116062; Thermo Fisher Scientific), R10G (1/500; 011-25811; FUJIFILM Wako Pure Chemical), or α-actinin (1/800; A7811-.2 ML; Sigma-Aldrich, St. Louis, MO, USA). Next, 0.1% Tween 20 (Sigma-Aldrich) was added to assess nuclear targets (brachyury and Nkx2.5), and then the supernatant was removed. The cells were washed with DPBS (−) containing 0.1% Tween 20 thrice and incubated with goat antimouse IgG Alexa Fluor 488 (1/2000; A-11001; Thermo Fisher Scientific), goat anti-rabbit IgG H&L Alexa Fluor 488 (1/1000; ab150077; abcam, Cambridge, U.K.), goat anti-rabbit IgG H&L Alexa Fluor 594 (1/1000; ab150080; abcam), or donkey anti-goat IgG H&L Alexa Fluor 488 (1/1000; ab150129; abcam) at 25 °C for 1 h. After washing with DPBS (−) containing 0.1% Tween 20 three times, the cells were stained with 1 μg/mL 4′,6-diamidino-2-phenylindole (DAPI; FUJIFILM Wako Pure Chemical) for 20 min and washed again with DPBS (−) containing 0.1% Tween 20. Cells in 24-well plates were examined under a microscope, Eclipse Ts2 (Nikon, Tokyo, Japan), at 594, 488, and 385 nm for differentiation-specific and nuclear markers, respectively. Cell counting on day 6 was based on the number of DAPI-positive cells.

5.3. Protein Preparation for LC/MS/MS. The cells (days 0, 1, 2, 3, 5, 7, 10, 12, and 18) were washed twice with DPBS (−) and mixed in buffer D[52] comprising 12 mM sodium deoxycholate, 12 mM *N*-lauroylsarcosine, and 100 mM Tris-

https://doi.org/10.1021/acsomega.4c06371
ACS Omega 2025, 10, 344−357

HCl, pH 9.0. The cell lysate was collected and incubated at 95 °C for 5 min. The samples were sonicated to remove the viscous matter. Protein concentration was determined using a bicyclohexoninic acid (BCA) protein assay. Subsequently, 100 μg of protein was diluted to 1.0 μg/μL in dissolution buffer D. The proteins were reduced by incubation with 10 mM 2-mercaptoethanol (FUJIFILM Wako Pure Chemical) at 37 °C for 30 min. Alkylation was performed by incubation with 20 mM acrylamide (FUJIFILM Wako Pure Chemical) at 37 °C in the dark for 60 min. The protein solution was incubated with 1 μg of lysyl endopeptidase mass spectrometry grade (FUJIFILM Wako Pure Chemical) at 37 °C for 60 min. Next, 50 mM Tris-HCl, pH 8.5, containing 1.5 mM $CaCl_2$ was added with 2 μg of trypsin (FUJIFILM Wako Pure Chemical) and cell lysate was incubated at 37 °C for 16 h. The reaction was terminated by adding 500 μL of ethyl acetate, followed by 10 μL of formic acid. After stirring and centrifugation at 14 000*g*, the supernatant was discarded. Desalting was performed using an Oasis PRiME HLB 1 cc Extraction Cartridge (Waters Corporation, Milford, CA, USA) following the manufacturer's instructions. The protein fraction was dried using a Speed Vac concentrator (Sakuma, Tokyo, Japan), and the dried sample was reconstituted with 0.1% formic acid/3% acetonitrile (ACN) to a final concentration of 0.1 μg/μL proteins.

5.4. LC/MS/MS. Briefly, 0.1 μg of the peptides was analyzed using an LC/MS/MS instrument comprising Q-Exactive (Thermo Fisher Scientific) and EASY-nLC1000 (Thermo Fisher Scientific) equipped with an Acclaim PepMapC18 (3 μm, 0.075 mm × 10 mm; Thermo Fisher Science) column and an NTCC-360/75-3-125 (C18, 3 μm, 0.075 mm × 125 mm; Nikkyo Technos, Tokyo, Japan) column. Solvent A was 0.1% formic acid, and solvent B was acetonitrile with 0.1% formic acid. Separation was performed using a gradient eluent (0−35% linear gradient of solvent B at 0−150 min, 35−100% of solvent B at 150−151 min, and 100% of solvent B at 151−155 min) at a flow rate of 300 nL/min.

The mass spectrometer was operated in DIA-MS mode. Data were acquired in positive ion mode with a spray voltage of 1800 V and fragmentation by high-energy collision dissociation. The Q-Exactive method was the same as previously reported.[24]

5.5. Quantitative Proteomics. A database search was performed using DIA-NN[53] against the UniProt Human Database (March 2021). Raw data were converted into mzml format in ProteoWizard (3.0.21).[54] mzml data were converted to dia data using DIA-NN. The protease was Trypsin/P, and missed cleavage was 1. The box for N-term M excision and C carbamidomethylation was checked. The peptide length range was 7−30. The precursor charge range was 1−4. The precursor m/z range was 495−905. The fragment ion m/z range was 100−1800. Precursor false discovery rate was 1.0%.

5.6. RNAi. Opti-MEM (Thermo Fisher Scientific) and Lipofectamine RNAiMAX (Thermo Fisher Scientific) were mixed in a ratio of 50:3. Opti-MEM and 10 μM siRNA (Silencer Select siRNA TPBG, Silencer Select Negative Control) were mixed in a ratio of 50:1. Equal amounts of the two mixtures were combined to prepare the siRNA solutions. hiPSCs were seeded in 6-well plates, and cardiac differentiation was induced for 5 days. On days 5 and 6, the cells were transfected with siRNA by adding the siRNA solution to a final concentration of 10 nM. At day 7, the cells were harvested.

5.7. Flow Cytometric Analysis. On day 18 of differentiation, cells were washed twice with DPBS (−) and incubated in TrypLE (Thermo Fisher Scientific) at 37 °C for 10 min to detach. The cells were then centrifuged at 300*g* for 4 min, the supernatant was removed, and the cells were incubated with 99.8% methanol at 4 °C for 20 min. The cells were rinsed twice with 0.5% BSA/DPBS (−)/0.5 mM EDTA. After removing the solution, the cells were incubated in 0.5% BSA/DPBS (−)/0.5 mM EDTA with anticardiac troponin T (1/20; 564767; BD Biosciences., Franklin Lakes, USA) antibodies at 4 °C for 1 h. The cells were washed twice with 0.5% BSA/DPBS (−)/0.5 mM EDTA, and aggregates were removed by filtration through a cell strainer (BD Falcon, New York, USA). The cells were examined using a CytoFLEX-S flow cytometer (Beckman Coulter, California, USA) at 488 nm at a flow rate of 10 μL/min; 10000 events were recorded for each sample. Data analysis was performed by using CytExpert.

5.8. Statistical Analysis. DIA-MS experiments were performed using six technical replicates. All DIA-MS data were analyzed by DIA-NN (1.8), and data sorting was performed by using Microsoft Excel. Data are expressed as the mean ± standard error. Data were analyzed using a two-tailed Student's t test. GO analysis was performed using Metascape (https://metascape.org/gp/index.html#/main/step1). Network analysis was performed using STRING (https://string-db.org/) (version 12.0). Pathway analysis was performed using the KEGG Mapper Color (https://www.genome.jp/kegg/mapper/color.html). Heatmap and clustering analyses were performed using Perseus software (version 1.6.13.0). Clustering analysis was performed by calculating abundance ratios based on day 0. Volcano plots were created using our script with pandas (version 1.2.3), NumPy (version 1.20.1), scikit-learn (version 0.24.2), seaborn (version 0.11.1), matplotlib (version 3.3.4), and bioinfokit (version 2.0.4). In the comparison of TPBG expression levels, normalization was performed so that the total ion chromatogram intensities were equal. For comparing control cells and TPBG-KD cells, normalization was performed so that the relative values of all proteins in the nontargeting control and TPBG-KD had the same mean value. For normalization, missing data were assigned the smallest identified value. PCA was performed using R software (version 4.2.0). Missing data were assigned a value of zero.

5.9. Data Availability. The data sets generated during and analyzed during the current study are available in the Japan Proteome Standard Repository, https://repository.jpostdb.org/ (PXD044846 and PXD056768). Proteome data on day 7 of differentiation into NSC were from our previous data deposited in Japan Proteome Standard Repository, https://repository.jpostdb.org/ (PXD034925).

■ ASSOCIATED CONTENT

Supporting Information

The Supporting Information is available free of charge at https://pubs.acs.org/doi/10.1021/acsomega.4c06371.

Movie S1 showing cells on day 8 of cardiac differentiation (MP4)

Movie S2 showing cardiomyocytes on day 18 of cardiac differentiation (MP4)

Movie S3 showing TPBG-KD cells on day 18 of cardiac differentiation (MP4)

https://doi.org/10.1021/acsomega.4c06371
ACS Omega 2025, 10, 344−357

Movie S4 showing WT cells on day 18 of cardiac differentiation (MP4)

Movie S5 showing control cells on day 18 of cardiac differentiation (MP4)

Table S1 of list of identified proteins and their peak areas; Table S2 of list of proteins used for PCA and their loadings; Table S3 of list of protein variations at each differentiation point used in the volcano plot; Table S4 of list of proteins changed by TPBG-KD; Table S5 of GO analysis of proteins up- and down-regulated by TPBG-KD (XLSX), Figure S1 showing characterization of 201B7-derived differentiating cells by immunostaining; Figure S2 showing characterization of 610B1-derived differentiating cells by immunostaining; Figure S3 showing clustering analysis reflecting all replication data; Figure S4 showing GO analysis of proteins showing an increase by volcano plot; Figure S5 showing GO analysis of proteins showing a decrease by volcano plot; Figure S6 showing network analysis of up-regulated proteins extracted by volcano plot; Figure S7 showing immunostaining analysis on day 7; Figure S8 showing immunostaining analysis of TPBG on days 0−18; Figure S9 showing effect of TPBG-KD transfected with TPBG-siRNA on day 5 and day 6 on protein expression (PDF)

AUTHOR INFORMATION

Corresponding Author

Nana Kawasaki − *Biopharmaceutical and Regenerative Sciences, Graduate School of Medical Life Science, Yokohama City University, Yokohama 230-0045, Japan;* orcid.org/0000-0002-5447-1890; Email: nana@yokohama-cu.ac.jp

Author

Takaya Urasawa − *Biopharmaceutical and Regenerative Sciences, Graduate School of Medical Life Science, Yokohama City University, Yokohama 230-0045, Japan*

Complete contact information is available at: https://pubs.acs.org/10.1021/acsomega.4c06371

Author Contributions

N.K. and T.U.: study design, funding acquisition, and manuscript writing. N.K.: project administration. T.U.: experiments, statistical analysis, and visualization.

Funding

This study was supported by JSPS KAKENHI Grant JP21H02617 (to N.K.), a Grant-in-Aid (Grant IBUNNYAYU-GO) provided by Kanagawa Prefectural Government for Integration of Advanced Multidisciplinary Research Activity (to N.K.), a grant for 2021−2023 Strategic Research Promotion (Grant SK3001) of Yokohama City University (to N.K.), and JST and the establishment of university fellowships toward the creation of science technology innovation, Grant JPMJFS2140 (to T.U.).

Notes

The authors declare no competing financial interest.

ACKNOWLEDGMENTS

The authors thank Dr. Toru Sugawara and Dr. Daisuke Takakura (Yokohama City University) for useful discussions and are grateful to Dr. Yoji Sato and Dr. Takuya Kuroda (National Institute of Health Sciences) for helpful comments. The authors thank Editage (www.editage.com) and Enago (www.enago.com) for English language editing.

REFERENCES

(1) Takahashi, K.; Yamanaka, S. Induction of pluripotent stem cells from mouse embryonic and adult fibroblast cultures by defined factors. *Cell* **2006**, *126*, 663−676.

(2) Takahashi, J. Stem cells and regenerative medicine for neural repair. *Curr. Opin. Biotechnol.* **2018**, *52*, 102−108.

(3) Deguchi, S.; Takayama, K.; Mizuguchi, H. Generation of human induced pluripotent stem cell-derived hepatocyte-like cells for cellular medicine. *Biol. Pharm. Bull.* **2020**, *43*, 608−615.

(4) Kikuchi, T.; Morizane, A.; Doi, D.; Magotani, H.; Onoe, H.; Hayashi, T.; Mizuma, H.; Takara, S.; Takahashi, R.; Inoue, H.; Morita, S.; et al. Human iPS cell-derived dopaminergic neurons function in a primate Parkinson's disease model. *Nature* **2017**, *548*, 592−596.

(5) Kim, C. iPSC technology–Powerful hand for disease modeling and therapeutic screen. *BMB Rep.* **2015**, *48*, 256−265.

(6) Silva, M. C.; Haggarty, S. J. Human pluripotent stem cell-derived models and drug screening in CNS precision medicine. *Ann. N.Y. Acad. Sci.* **2020**, *1471*, 18−56.

(7) Egawa, N.; Kitaoka, S.; Tsukita, K.; Naitoh, M.; Takahashi, K.; Yamamoto, T.; Adachi, F.; Kondo, T.; Okita, K.; Asaka, I.; Aoi, T.; et al. Drug screening for ALS using patient-specific induced pluripotent stem cells. *Sci. Transl. Med.* **2012**, *4*, No. 145ra104.

(8) Raya, A.; Rodríguez-Pizà, I.; Guenechea, G.; Vassena, R.; Navarro, S.; Barrero, M. J.; Consiglio, A.; Castellà, M.; Río, P.; Sleep, E.; González, F.; et al. Disease-corrected haematopoietic progenitors from Fanconi anaemia induced pluripotent stem cells. *Nature* **2009**, *460*, 53−59.

(9) Richard, J.-P.; Maragakis, N. J. Induced pluripotent stem cells from ALS patients for disease modeling. *Brain Res.* **2015**, *1607*, 15−25.

(10) Mahairaki, V.; Ryu, J.; Peters, A.; Chang, Q.; Li, T.; Park, T. S.; Burridge, P. W.; Talbot, C. C., Jr.; Asnaghi, L.; Martin, L. J.; Zambidis, E. T.; Koliatsos, V. E. Induced pluripotent stem cells from familial Alzheimer's disease patients differentiate into mature neurons with amyloidogenic properties. *Stem Cells Dev.* **2014**, *23*, 2996−3010.

(11) Miyagawa, S.; Kainuma, S.; Kawamura, T.; Suzuki, K.; Ito, Y.; Iseoka, H.; Ito, E.; Takeda, M.; Sasai, M.; Mochizuki-Oda, N.; Shimamoto, T.; et al. Case report: Transplantation of human induced pluripotent stem cell-derived cardiomyocyte patches for ischemic cardiomyopathy. *Front. Cardiovasc. Med.* **2022**, *9*, No. 950829.

(12) Tohyama, S.; Fujita, J.; Fujita, C.; Yamaguchi, M.; Kanaami, S.; Ohno, R.; Sakamoto, K.; Kodama, M.; Kurokawa, J.; Kanazawa, H.; Seki, T.; et al. Efficient large-scale 2D culture system for human induced pluripotent stem cells and differentiated cardiomyocytes. *Stem Cell Rep.* **2017**, *9*, 1406−1414.

(13) Wee, H.; Koo, K.; Bae, E.; Lee, T. Quality by design approaches to assessing the robustness of tangential flow filtration for MAb. *Biologicals* **2020**, *63*, 53−61.

(14) International Council for Harmonisation of Technical Requirements for Pharmaceuticals for Human Use "PHARMACEUTICAL DEVELOPMENT Q8 (R2)". https://database.ich.org/sites/default/files/Q8%28R2%29%20Guideline.pdf (2009).

(15) International Council for Harmonisation of Technical Requirements for Pharmaceuticals for Human Use "QUALITY RISK MANAGEMENT". https://database.ich.org/sites/default/files/Q9_Guideline.pdf (2005).

(16) International Council for Harmonisation of Technical Requirements for Pharmaceuticals for Human Use "PHARMACEUTICAL QUALITY SYSTEM". https://database.ich.org/sites/default/files/Q10%20Guideline.pdf (2008).

(17) International Council for Harmonisation of Technical Requirements for Pharmaceuticals for Human Use "DEVELOPMENT AND MANUFACTURE OF DRUG SUBSTANCES (CHEMICAL ENTITIES AND BIOTECHNOLOGICAL/BIOLOGICAL ENTITIES)

Q11". https://database.ich.org/sites/default/files/Q11%20Guideline.pdf (2012).
(18) Hirono, K.; Udugama, I. A.; Hayashi, Y.; Kino-oka, M.; Sugiyama, H. A dynamic and probabilistic design space determination method for mesenchymal stem cell cultivation processes. *Ind. Eng. Chem. Res.* **2022**, *61*, 7009−7019.
(19) Demmon, S.; Bhargava, S.; Ciolek, D.; Halley, J.; Jaya, N.; Joubert, M. K.; Koepf, E.; Smith, P.; Trexler-Schmidt, M.; Tsai, P. A cross-industry forum on benchmarking critical quality attribute identification and linkage to process characterization studies. *Biologicals* **2020**, *67*, 9−20.
(20) Thakur, S. S.; Geiger, T.; Chatterjee, B.; Bandilla, P.; Fröhlich, F.; Cox, J.; Mann, M. Deep and highly sensitive proteome coverage by LC-MS/MS without prefractionation. *Mol. Cell Proteomics* **2011**, *10*, No. M110.003699.
(21) Hofsteen, P.; Robitaille, A. M.; Chapman, D. P.; Moon, R. T.; Murry, C. E. Quantitative proteomics identify DAB2 as a cardiac developmental regulator that inhibits WNT/β-catenin signaling. *Proc. Natl. Acad. Sci. U. S. A.* **2016**, *113* (4), 1002−1007.
(22) Cai, W.; Zhang, J.; de Lange, W. J.; Gregorich, Z. R.; Karp, H.; Farrell, E. T.; Mitchell, S. D.; Tucholski, T.; Lin, Z.; Biermann, M.; et al. An unbiased proteomics method to assess the maturation of human pluripotent stem cell-derived cardiomyocytes. *Circ. Res.* **2019**, *125* (11), 936−953.
(23) Gillet, L. C.; Navarro, P.; Tate, S.; Rost, H.; Selevsek, N.; Reiter, L.; Bonner, R.; Aebersold, R. Targeted data extraction of the MS/MS spectra generated by data-independent acquisition: a new concept for consistent and accurate proteome analysis. *Mol. Cell. Proteomics* **2012**, *11*, O111.016717.
(24) Urasawa, T.; Koizumi, T.; Kimura, K.; Ohta, Y.; Kawasaki, N. Quantitative proteomics for the development and manufacturing of human-induced pluripotent stem cell-derived neural stem cells using data-independent acquisition mass spectrometry. *J. Proteome Res.* **2023**, *22* (6), 1843−1854.
(25) Zhang, F.; Ge, W.; Huang, L.; Li, D.; Liu, L.; Dong, Z.; Xu, L.; Ding, X.; Zhang, C.; Sun, Y.; Jun, A.; et al. A comparative analysis of data analysis tools for data-independent acquisition mass spectrometry. *Mol. Cell Proteomics* **2023**, *22*, No. 100623.
(26) Takeda, M.; Kanki, Y.; Masumoto, H.; Funakoshi, S.; Hatani, T.; Fukushima, H.; Izumi-Taguchi, A.; Matsui, Y.; Shimamura, T.; Yoshida, Y.; Yamashita, J. K. Identification of cardiomyocyte-fated progenitors from human-induced pluripotent stem cells marked with CD82. *Cell Rep.* **2018**, *22*, 546−556.
(27) Xu, C.; Zhao, H.; Chen, H.; Yao, Q. CXCR4 in breast cancer: oncogenic role and therapeutic targeting. *Drug Des. Dev. Ther.* **2015**, *9*, 4953−4964.
(28) Frame, M. C. Src in cancer: deregulation and consequences for cell behaviour. *Biochim. Biophys. Acta* **2002**, *1602*, 114−130.
(29) Cheng, Y.; Qu, J.; Che, X.; Xu, L.; Song, N.; Ma, Y.; Gong, J.; Qu, X.; Liu, Y. CXCL12/SDF-1α induces migration via SRC-mediated CXCR4-EGFR cross-talk in gastric cancer cells. *Oncol. Lett.* **2017**, *14*, 2103−2110.
(30) Sato, S.; Ishikawa, H.; Yoshikawa, H.; Izumikawa, K.; Simpson, R. J.; Takahashi, N. Collaborator of alternative reading frame protein (CARF) regulates early processing of pre-ribosomal RNA by retaining XRN2 (5′-3′ exoribonuclease) in the nucleoplasm. *Nucleic Acids Res.* **2015**, *43* (21), 10397−10410.
(31) Ward, C. M.; Barrow, K.; Woods, A. M.; Stern, P. L. The 5T4 oncofoetal antigen is an early differentiation marker of mouse ES cells and its absence is a useful means to assess pluripotency. *J. Cell Sci.* **2003**, *116*, 4533−4542.
(32) Eastham, A. M.; Spencer, H.; Soncin, F.; Ritson, S.; Merry, C. L.; Stern, P. L.; Ward, C. M. Epithelial-mesenchymal transition events during human embryonic stem cell differentiation. *Cancer Res.* **2007**, *67*, 11254−11262.
(33) Spencer, H. L.; Eastham, A. M.; Merry, C. L.; Southgate, T. D.; Perez-Campo, F.; Soncin, F.; Ritson, S.; Kemler, R.; Stern, P. L.; Ward, C. M. E-cadherin inhibits cell surface localization of the pro-migratory 5T4 oncofetal antigen in mouse embryonic stem cells. *Mol. Biol. Cell* **2007**, *18*, 2838−2851.
(34) Southgate, T. D.; McGinn, O. J.; Castro, F. V.; Rutkowski, A. J.; Al-Muftah, M.; Marinov, G.; Smethurst, G. J.; Shaw, D.; Ward, C. M.; Miller, C. J.; et al. CXCR4 mediated chemotaxis is regulated by 5T4 oncofetal glycoprotein in mouse embryonic cells. *PLoS One* **2010**, *5*, No. e9982.
(35) Liu, Z.; Zhang, Q. B.; Bu, C.; Wang, D.; Yu, K.; Gan, Z.; Chang, J.; Cheng, Z.; Liu, Z. Quantitative Dynamics of Proteome, Acetylome, and Succinylome during Stem-Cell Differentiation into Hepatocyte-like Cells. *J. Proteome Res.* **2018**, *17* (7), 2491−2498.
(36) Chu, L. F.; Leng, N.; Zhang, J.; Hou, Z.; Mamott, D.; Vereide, D. T.; Choi, J.; Kendziorski, C.; Stewart, R.; Thomson, J. A. Single-cell RNA-seq reveals novel regulators of human embryonic stem cell differentiation to definitive endoderm. *Genome Biol.* **2016**, *17* (1), 173.
(37) Kagermeier-Schenk, B.; Wehner, D.; Ozhan-Kizil, G.; Yamamoto, H.; Li, J.; Kirchner, K.; Hoffmann, C.; Stern, P.; Kikuchi, A.; Schambony, A.; Weidinger, G. Waif1/5T4 inhibits Wnt/β-catenin signaling and activates noncanonical Wnt pathways by modifying LRP6 subcellular localization. *Dev. Cell* **2011**, *21*, 1129−1143.
(38) Stern, P. L.; Brazzatti, J.; Sawan, S.; McGinn, O. J. Understanding and exploiting 5T4 oncofoetal glycoprotein expression. *Semin. Cancer Biol.* **2014**, *29*, 13−20.
(39) Park, S.; Yoo, J. E.; Yeon, G. B.; Kim, J. H.; Lee, J. S.; Choi, S. K.; Hwang, Y. G.; Park, C. W.; Cho, M. S.; Kim, J.; Na, D.; et al. Trophoblast glycoprotein is a new candidate gene for Parkinson's disease. *npj. Parkinson's Dis.* **2021**, *7*, 110.
(40) Lian, X.; Hsiao, C.; Wilson, G.; Zhu, K.; Hazeltine, L. B.; Azarin, S. M.; Raval, K. K.; Zhang, J.; Kamp, T. J.; Palecek, S. P. Robust cardiomyocyte differentiation from human pluripotent stem cells via temporal modulation of canonical Wnt signaling. *Proc. Natl. Acad. Sci. U. S. A.* **2012**, *109*, No. E1848.
(41) Kadari, A.; Mekala, S.; Wagner, N.; Malan, D.; Köth, J.; Doll, K.; Stappert, L.; Eckert, D.; Peitz, M.; Matthes, J.; Sasse, P.; et al. Robust generation of cardiomyocytes from human iPS cells requires precise modulation of BMP and WNT signaling. *Stem Cell Rev. Rep.* **2015**, *11*, 560−569.
(42) Ozhan, G.; Weidinger, G. Wnt/β-catenin signaling in heart regeneration. *Cell Regener.* **2015**, *4* (1), 3.
(43) Gessert, S.; Kühl, M. The multiple phases and faces of wnt signaling during cardiac differentiation and development. *Circ. Res.* **2010**, *107*, 186−199.
(44) Lian, X.; Zhang, J.; Azarin, S. M.; Zhu, K.; Hazeltine, L. B.; Bao, X.; Hsiao, C.; Kamp, T. J.; Palecek, S. P. Directed cardiomyocyte differentiation from human pluripotent stem cells by modulating Wnt/β-catenin signaling under fully defined conditions. *Nat. Protoc.* **2013**, *8*, 162−175.
(45) Wolling, H.; Konze, S. A.; Höfer, A.; Erdmann, J.; Pich, A.; Zweigerdt, R.; Buettner, F. F. R. Quantitative Secretomics Reveals Extrinsic Signals Involved in Human Pluripotent Stem Cell Cardiomyogenesis. *Proteomics* **2018**, *18* (14), No. e1800102.
(46) Min, J. K.; Park, H. S.; Lee, Y. B.; Kim, J. G.; Kim, J. I.; Park, J. B. Cross-talk between wnt signaling and Src tyrosine kinase. *Biomedicines* **2022**, *10* (5), 1112.
(47) Vadlakonda, L.; Pasupuleti, M.; Pallu, R. Role of PI3K-AKT-mTOR and Wnt signaling pathways in transition of G1-S phase of cell cycle in cancer cells. *Front. Oncol.* **2013**, *3*, 85.
(48) Niehrs, C.; Acebron, S. P. Mitotic and mitogenic Wnt signalling. *EMBO J.* **2012**, *31*, 2705−2713.
(49) Stavish, D.; Böiers, C.; Price, C.; Frith, T. J. R.; Halliwell, J.; Saldaña-Guerrero, I.; Wray, J.; Brown, J.; Carr, J.; James, C.; Barbaric, I.; et al. Generation and trapping of a mesoderm biased state of human pluripotency. *Nat. Commun.* **2020**, *11*, 4989.
(50) Halloin, C.; Schwanke, K.; Löbel, W.; Franke, A.; Szepes, M.; Biswanath, S.; Wunderlich, S.; Merkert, S.; Weber, N.; Osten, F.; de la Roche, J.; et al. Continuous WNT control enables advanced hPSC

https://doi.org/10.1021/acsomega.4c06371
ACS Omega 2025, 10, 344−357

cardiac processing and prognostic surface marker identification in chemically defined suspension culture. *Stem Cell Rep.* **2019**, *13*, 775.
(51) Burridge, P. W.; Holmström, A.; Wu, J. C. Chemically defined culture and cardiomyocyte differentiation of human pluripotent stem cells. *Curr. Protoc. Hum. Genet.* **2015**, *87*, 21.
(52) Masuda, T.; Ishihama, Y. Sample preparation for shotgun proteomics by using phase transfer surfactants. *Proteome Lett.* **2016**, *1*, 95−100.
(53) Demichev, V.; Messner, C. B.; Lilley, K. S.; Ralser, M. DIA-NN: Deep neural networks substantially improve the identification performance of Data-independent acquisition (DIA) in proteomics. *bioRxiv* **2018**, No. 282699.
(54) Chambers, M. C.; Maclean, B.; Burke, R.; Amodei, D.; Ruderman, D. L.; Neumann, S.; Gatto, L.; Fischer, B.; Pratt, B.; Egertson, J.; Hoff, K.; et al. A cross-platform toolkit for mass spectrometry and proteomics. *Nat. Biotechnol.* **2012**, *30*, 918−920.

https://doi.org/10.1021/acsomega.4c06371
ACS Omega 2025, 10, 344−357